Electronic Supporting Information (ESI)

Engineered Water-soluble Two-dimensional Magnetic Nanocomposites: Towards High Magnetic Relaxometric Properties

Erwin Peng[1], Fenghe Wang[1], Bingwen Zheng[2], Sam Fong Yau Li[2,3] and Jun Min Xue*[1]*

[1]Department of Materials Science and Engineering, Faculty of Engineering, National University of Singapore (NUS), 7 Engineering Drive 1, Singapore 117574.

*Email: msexuejm@nus.edu.sg and mseer@nus.edu.sg

[2]Department of Chemistry, National University of Singapore, 3 Science Drive 3, Singapore 117543.

[3]NUS Environment Research Institute (NERI), Department of Chemistry, 3 Science Drive 3, Singapore 117573.

S1. Basic Characterization of Graphene Oxide Sheets in Water

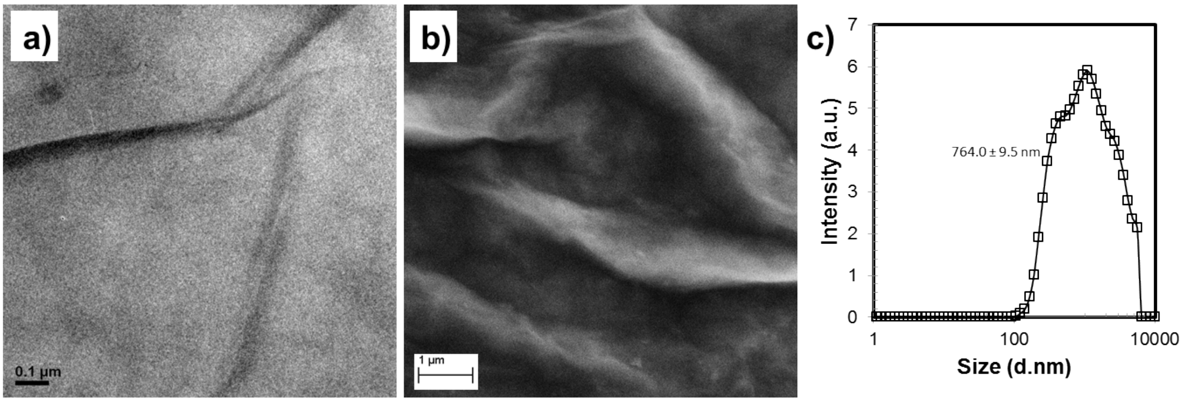

Fig. S1 (a) TEM and (b) SEM images of purchased graphene oxide (GO) solution from Graphene Supermarket. (c) Hydrodynamic size distribution of GO in water.

The as-purchased graphene oxide (GO) from Graphene Supermarket was characterized by TEM and SEM images (see **Fig. S1a,b**). From the microscopy images, two-dimensional sheet-like structure was observed with lateral dimension of more than few microns. However, the overall hydrodynamic size of the GO sheets in water was only 764.0 ± 9.5 nm (see **Fig. S1c**) as GO sheets will fold and assume crumpled configurations. GO sheets were very stable in aqueous phase due to the presence of hydrophilic functional groups such as epoxy, hydroxyls, carbonyls and carboxylic acid groups that provided electrostatic repulsion [1].

S2. Additional Data for MFN-18 Nanocomposites

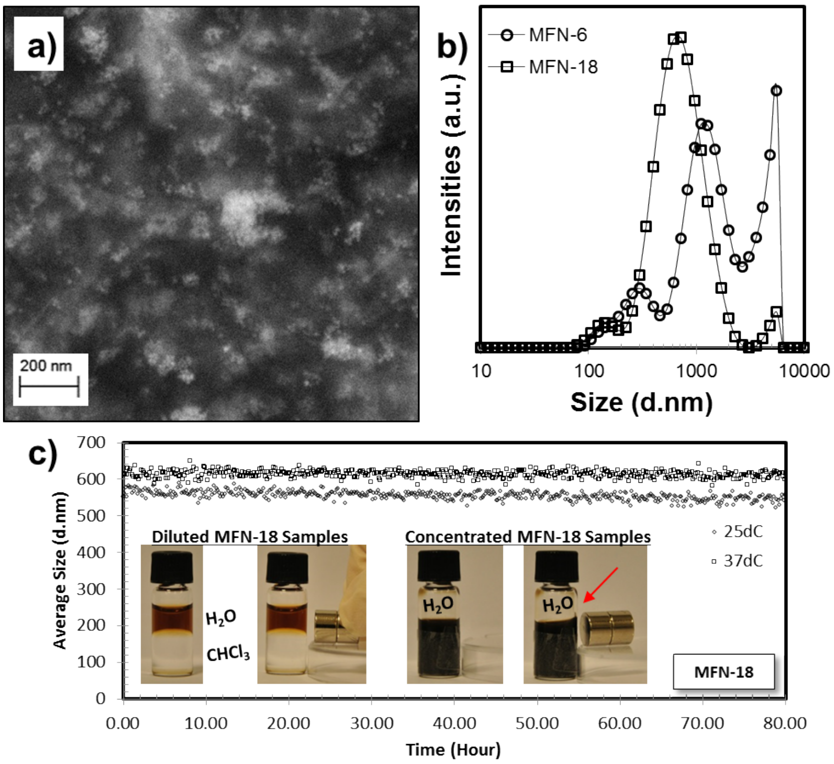

Fig. S2 (a) SEM image of MFN-18 in water. (b) Hydrodynamic size distributions of MFN-6 and MFN-18 in water at 25^{o}C from DLS measurement. (c) Time-dependent stability test of MFN-18 in water at both 25^{o}C and 37^{o}C.

The SEM image of MFN-18 was given in **Fig. S2a**. The average hydrodynamic sizes of MFN-6 and MFN-18 (size distribution was given in **Fig. S2b**) were 1224.8 ± 56.2 nm and 577.9 ± 10.7 nm, respectively. MFN-6 possessed larger hydrodynamic size as compared to MFN-18 due to the potential aggregation of MFP-6 nanoparticles in THF/water mixture as compared to MFP-18 (nano-sized effect in which MFP-6 possessed higher surface energy as compared to MFP-18 nanoparticles). The selective aggregation and deposition of these aggregates within GO sheets was due to the tendency of hydrophobic MNPs to aggregate (even when it was dispersed in water miscible solvent THF) when introduced to polar water solvent [2]. The time-dependent stability test was carried out on MFN-18 and the result demonstrated that MFN-18 was extremely stable in water. The average hydrodynamic sizes of MFN-18 in water at 25^{o}C and 37^{o}C during 86 hours incubation were 556.4 ± 11.2 nm and 614.8 ± 9.9 nm respectively (**Fig. S2c**). The inset of **Fig. S2c** demonstrated both the colloidal stability of dilute MFN-18 and concentrated MFN-18 samples in the presence of external magnetic field (table-top magnet). No separation of the MFN-18 sample from the water because of the magnetic field, indicating that the MFN-18 sample was very stable. For concentrated MFN-18 sample, the water-soluble nanocomposites formed perfect ferrofluid.

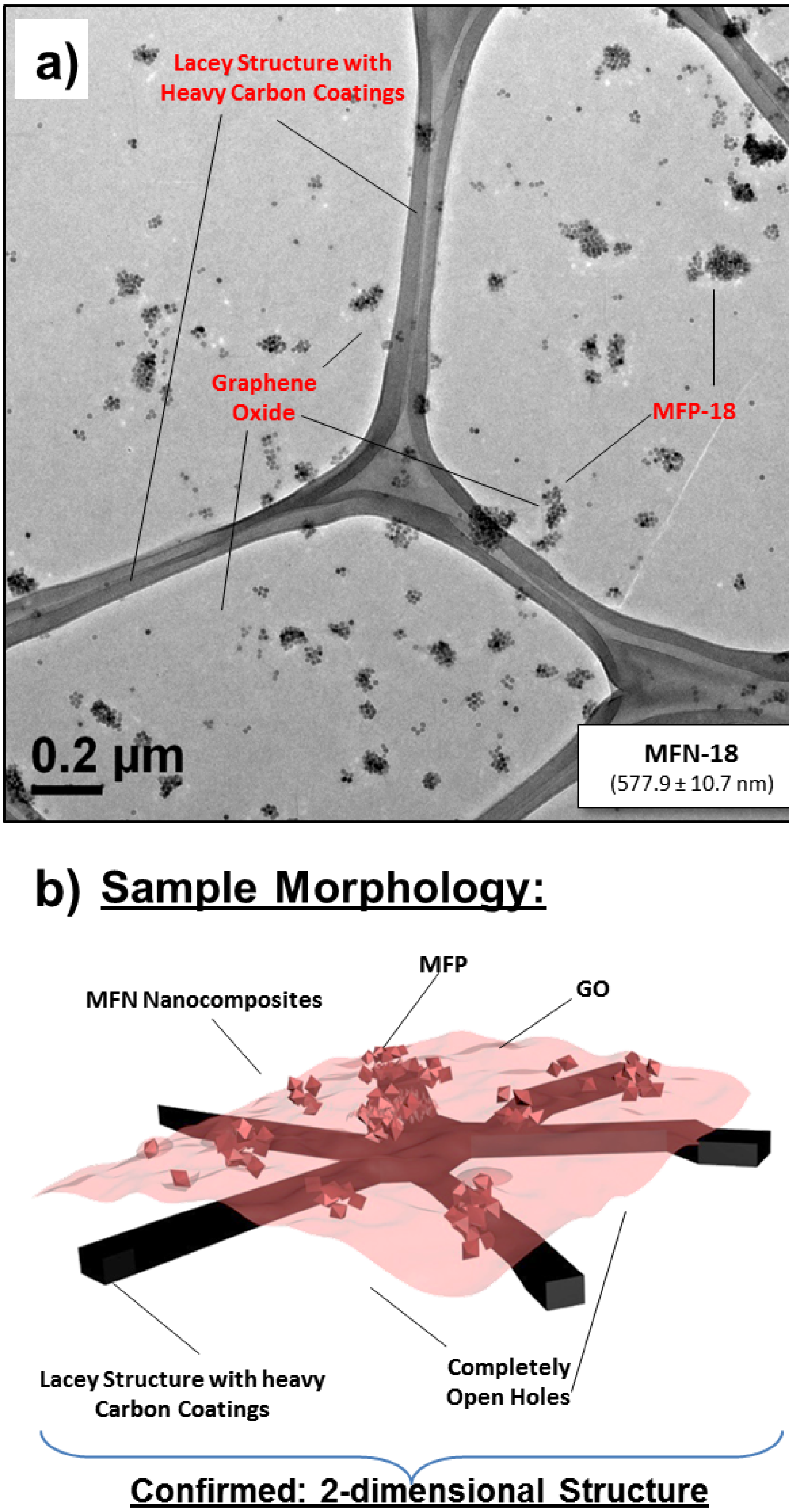

Fig. S3 (a) Low magnification TEM image of MFN-18 nanocomposites in water. The TEM sample was prepared with NetMesh^{TM} lacey formvar stabilized with carbon copper grid. The completely open holes structure with no film support was observed. (b) Illustration of MFN-18 sample with lacey formvar TEM grid.

The morphology of MFN-18 nanocomposite was also verified from the low magnification TEM image, taken on MFN-18 sample prepared with Lacey Formvar stabilized with Carbon (lacey structure enforced by heavy carbon coating). With completely open holes structure (see **Fig. S3a**), this TEM sample grid allowed viewing specimens without the interference from typical underlying support film materials. The fact that hydrophobic MFP-18 nanoparticles were observed within the open holes region indicated that the MFP-18 nanoparticles must be anchored onto the GO sheets. These GO sheets were then anchored onto the lacey structure of the lacey formvar. Based on the low magnification TEM image (see **Fig. S3a**), the SEM image (see **Fig. S2a**) and the typical TEM image (see **Fig. 1d**) of MFN-18 nanocomposite, the resultant morphology can be best depicted from the illustration given in **Fig. S3b**. Briefly, MFN-18 nanocomposite can be regarded as two-dimensional structure with hydrophobic MFP-18 nanoparticles were selectively deposited onto the hydrophobic region of the GO sheets. As the MFP-18 nanoparticles originally were hydrophobic due to oleic-acid surface coating, MFP-18 nanoparticles should be residing within the hydrophobic region of the two-dimensional nanocomposites. Therefore, this partial deposition (due to DSE method used) created hydrophobic/hydrophilic regions separation in which the hydrophilic region consisted of hydrophilic functional group of GO sheets such as hydroxyls, epoxy, carbonyl and carboxylic acid functional groups that helped to stabilized the nanocomposites in water.

S3. MRI T_1 Relaxivity of Samples with MFP-18 Cores

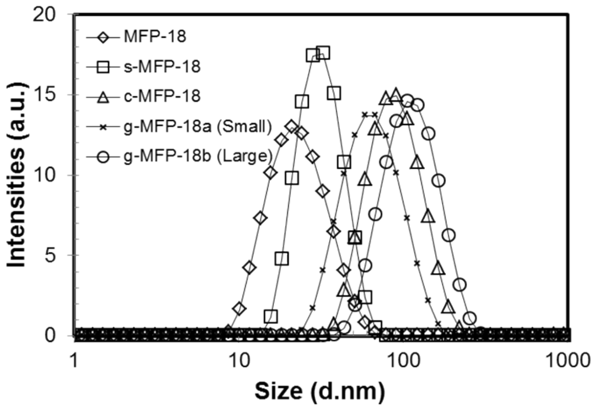

Fig. S4 Hydrodynamic size distributions of hydrophobic MFP-18 nanoparticles in CHCl3 as well as hydrophilic s-MFP-18, c-MFP-18, g-MFP-18a and g-MFP-18b nanocomposites in water at 25^{o}C.

Besides MFN-18 sample, there were other four different nanocomposites prepared: (i) individually encapsulated MFP-18 using amphiphilic brush copolymers PIMA-*g*-C_{12} (**s-MFP-18**; d_{hyd} = 29.5 nm), (ii) collectively encapsulated MFP-18 using amphiphilic brush copolymers PMAO-*g*-PEG (**c-MFP-18**; d_{hyd} = 82.9 nm), (iii) collectively encapsulated MFP-18 using GO/oleylamine complex (**g-MFP-18a,b**; d_{hyd} = 59.1 nm and 101.8 nm respectively) were also fabricated with two different GO sizes, simply by varying sonication time. The hydrodynamic size distribution of each aforementioned sample was plotted in **Fig. S4**.

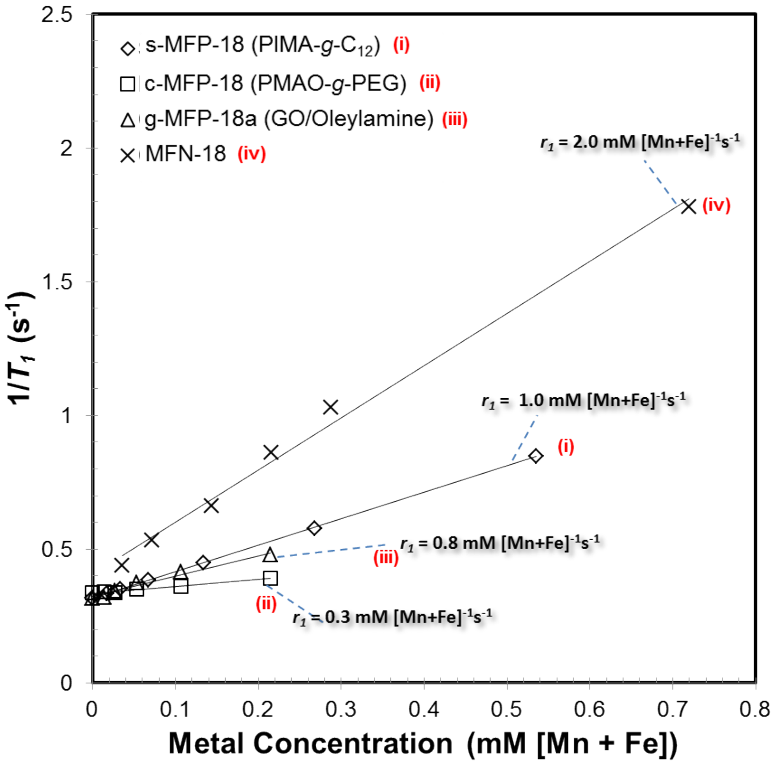

Fig. S5 Plot of longitudinal relaxation rate (1/T_1) of water-dispersible samples with MFP-18 cores: (i) s-MFP-18 (individually coated with PIMA-*g*-C_{12}), (ii) c-MFP-18 (collectively encapsulated with PMAO-*g*-PEG), (iii) g-MFP-18a (collectively encapsulated with GO/oleylamine complex) and (iv) decorated on GO sheets (MFN-18).

The summary of longitudinal relaxation rates (1/T_1) of MFP-18 samples with various surface coatings were presented in **Fig. S5**. The T_1 relaxivities of MFP-18 samples were rather weak, due to the strong susceptibility of MFP-18 cores. Overall, the r_1 values increased in the order of: **c-MFP-18 < g-MFP-18a < s-MFP-18 < MFN-18** samples. As both c-MFP-18 and g-MFP-18a samples fabrication relied on the use of mini-emulsion/solvent evaporation (MESE) technique to form the nanocomposites, aggregation of hydrophobic MFP-18 nanoparticles were expected and hydrophobic region (impermeable to water diffusion) was resulted. Both s-MFP-18 and MFN-18 samples demonstrated slightly higher r_1 values than c-MFP-18 and g-MFP-18a samples due to better water accessibility; resulting in better interaction between the metal ions of hydrophobic MFP-18 nanoparticles with the surrounding water protons. The overall model for MFN-18 sample that enhanced water accessibility and water retention can be best depicted by **Fig. S6**.

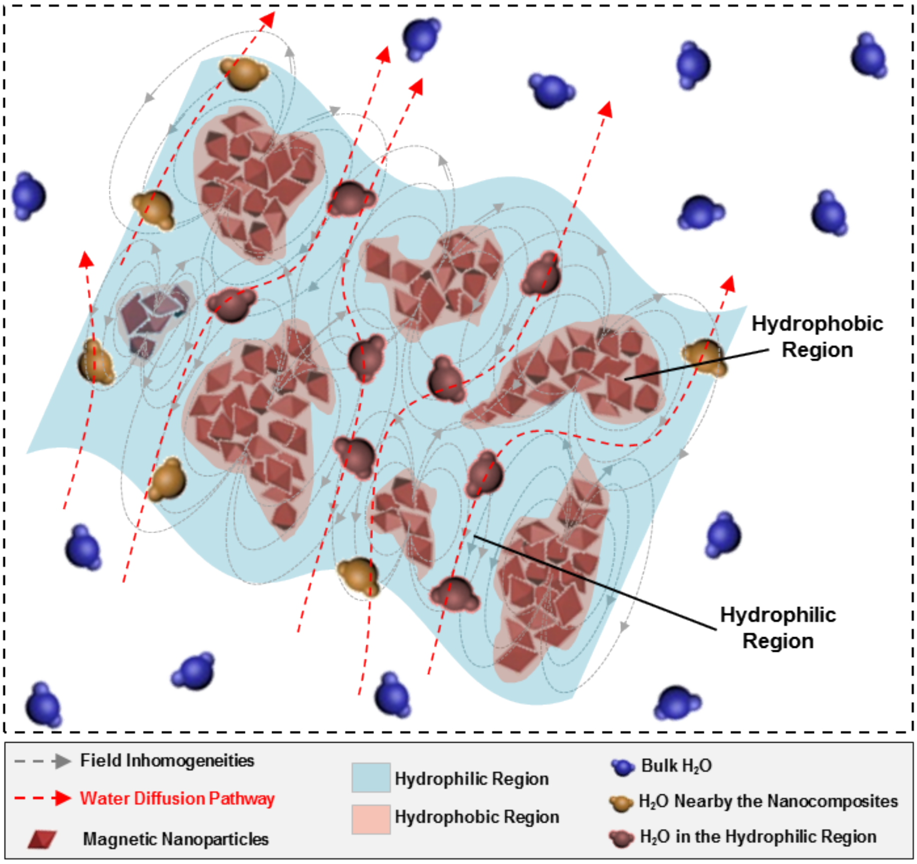

Fig. S6 Schematic diagram showing possible water diffusion pathway within the water-dispersible MFN-18 nanocomposites.

S4. Additional Data for ION-10

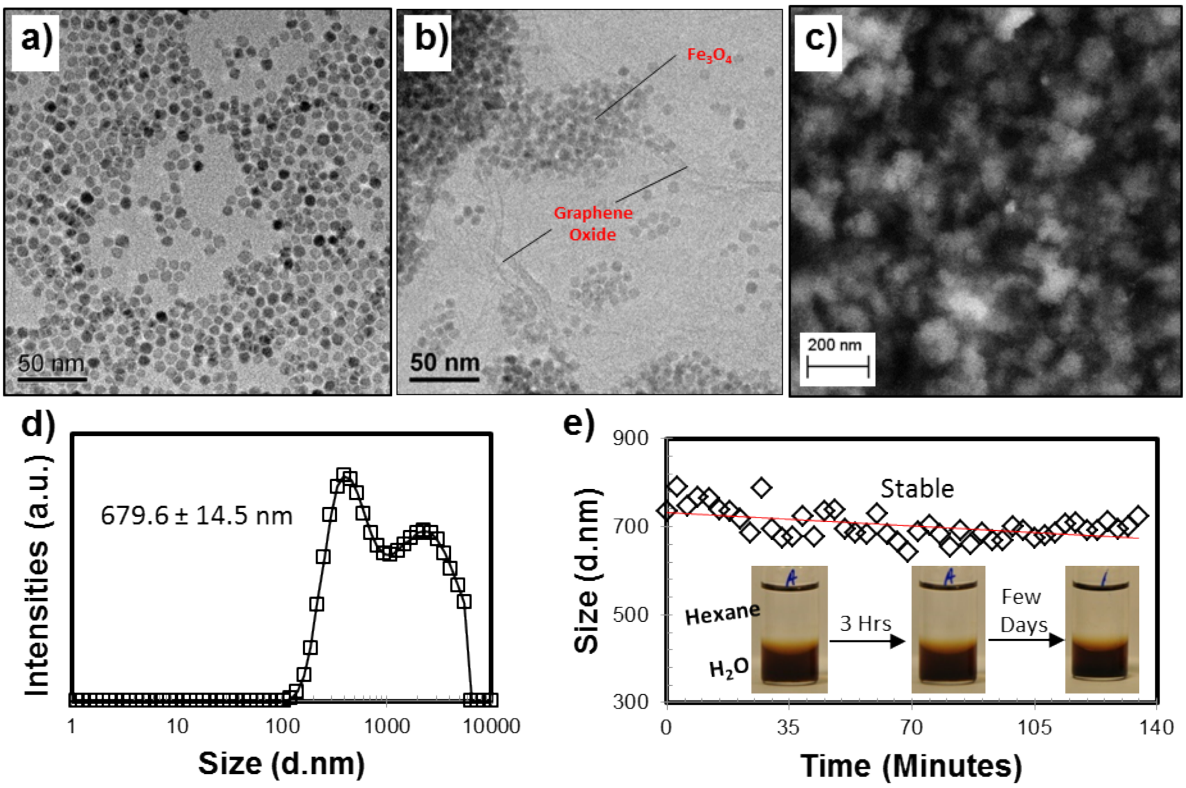

Fig. S7 (a) TEM image of IOP-10 nanoparticles in $CHCl_3$. (b) TEM image and (c) SEM image of ION-10 nanocomposites in water. (d) Hydrodynamic size distribution of ION-10 in water at 25°C from DLS measurement. (c) Time-dependent stability test of ION-10 in water at 25°C.

Similar to MFP-18, 10 nm Fe_3O_4 nanoparticles (IOP-10) were formed using similar thermal decomposition method of iron acetylacetonate $Fe(acac)_3$ in oleic acid and benzyl ether solvent. The original hydrophobic IOP-10 nanoparticles TEM image was given in **Fig. S7a**. Through the DSE approach, IOP-10 nanoparticles were selectively deposited onto two dimensional GO sheets, as confirmed from the TEM and SEM images in **Fig. S7b,c**. The average hydrodynamic size of ION-10 sample in water from DLS experiment (see **Fig. S7d**) was 679.6 ± 14.5 nm. Due to the presence of GO host, the nanocomposites ION-10 was inherently very stable in water (see the time-dependent d_{hyd} plot in **Fig. S7e**). The insets of **Fig. S7e** showed the digital photograph of IOP-10 samples in waters after 3 hours as well as after few days of incubation. During the incubation, hexane was presence on top of water phase. However, there was no observation on the re-dispersion of IOP-10 samples back onto non-polar phase.

The hydrophobic IOP-10 nanoparticles was also phase-transferred using GO/oleylamine host (MESE method, oleylamine as binder), two other samples **g-IOP-10a,b** were formed with different aggregate sizes (d_{hyd} of 138.4 nm and 182.3 nm) [3]. From the comparison given in **Fig. S8**, significant improvement over both transversal and longitudinal relaxation rate was observed for ION-10 sample over g-IOP-10a,b samples. This indicated that ION-10 construct has better hydration than g-IOP-10a,b structures where the hydrophobic oleylamine binder was presence on top of GO sheet (basal planes).

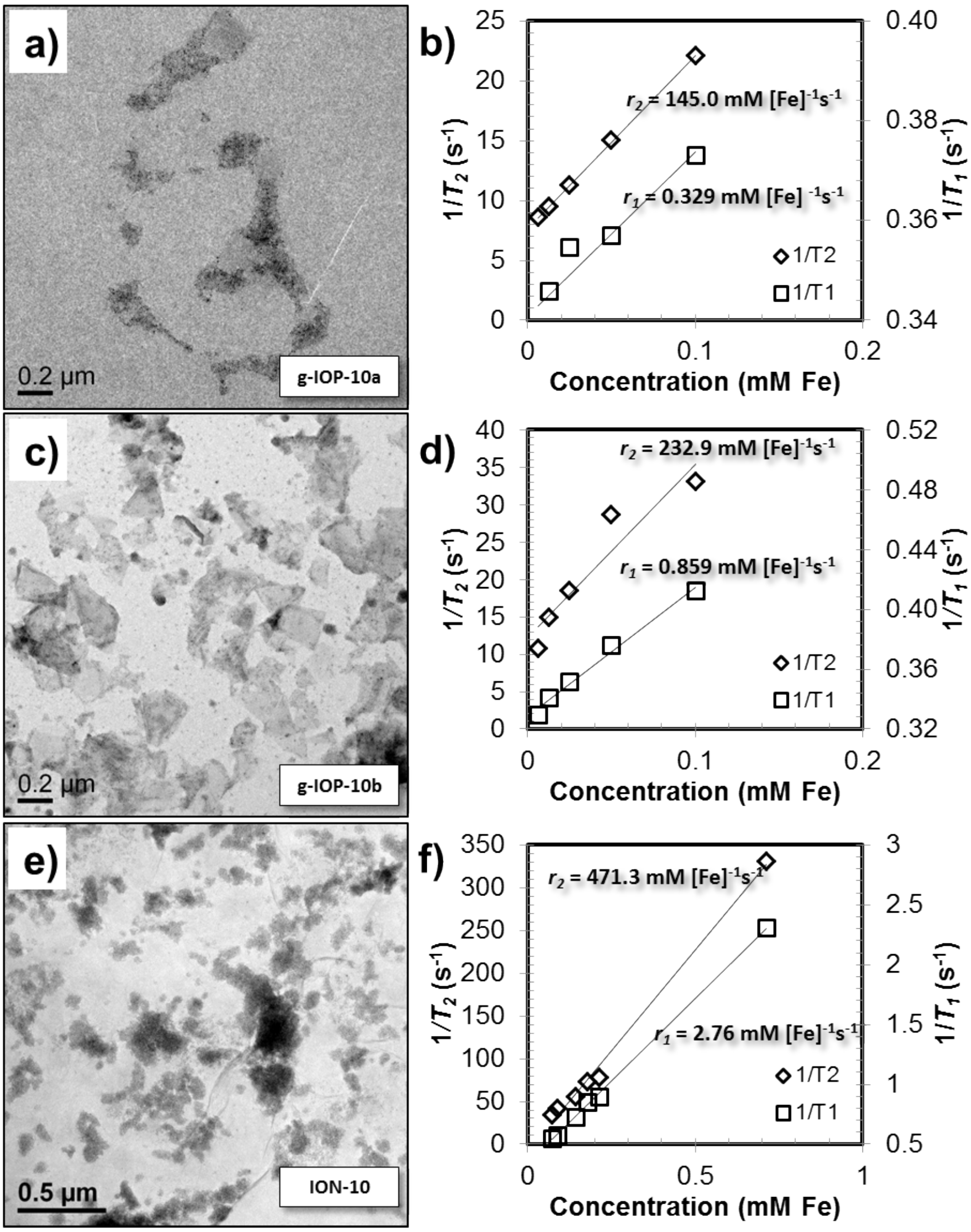

Fig. S8 (Left) TEM image and (Right) plot of T_1 and T_2 relaxation times of GO-based nanocomposites formed with 10 nm Fe_3O_4 nanoparticles (IOP-10) core: (a,b) g-IOP-10a, (c,d) g-IOP-10b, (e,f) ION-10.

S5. Formation of Smaller MFN-18* Nanocomposites

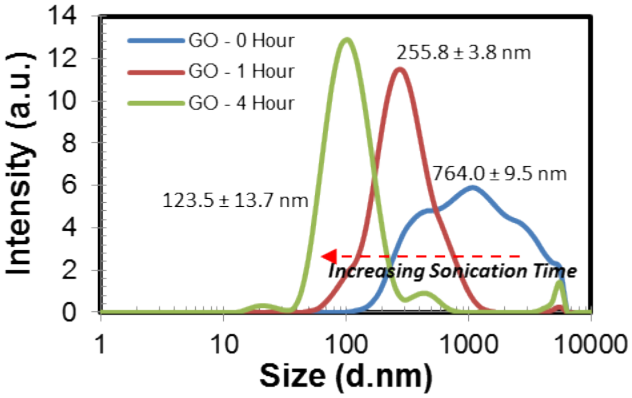

Fig. S9 Hydrodynamic size distribution of the as-purchased GO sheets with (a) 0 hour sonication, (b) 1 hour sonication and (4) hour sonication.

By sonicating the as-purchased GO sheets, the original d_{hyd} of GO at 764.0 ± 9.5 nm can be decreased to 255.8 ± 3.8 nm after 1 hour sonication and 123.5 ± 13.7 nm after 4 hours sonication process. During the sonication process using ultra-sonicator, GO broken up into smaller pieces and more surface defects especially in the basal plane of GO sheets were created. Because of this, the hydrophobic region became narrower while the hydrophilic region became wider, resulting in less aggregated MFP-18 nanoparticles after the formation of MFN-18* using pre-sonicated GO (as seen from **Fig. S10** below) as compared to MFN-18 nanocomposites (in **Fig.S3a**).

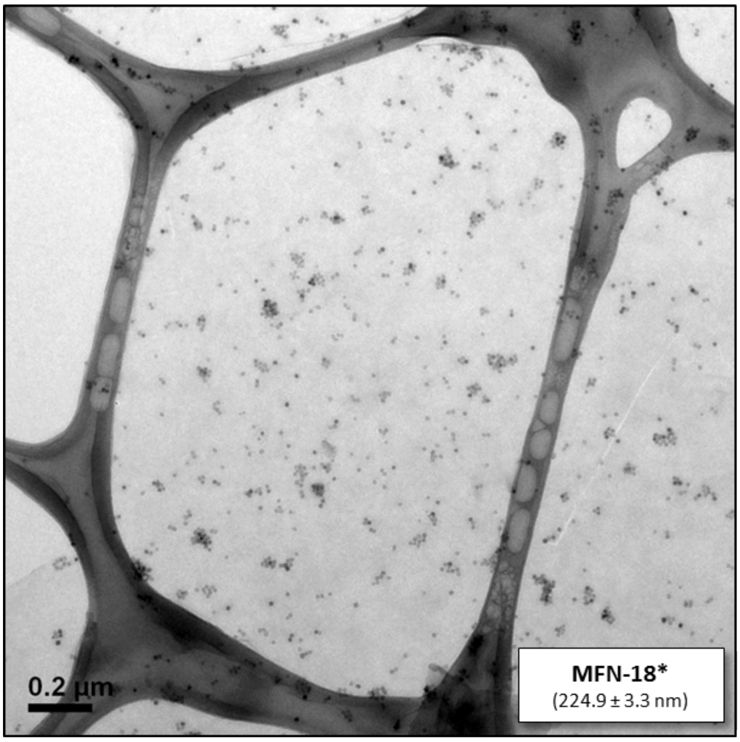

Fig. S10 Low magnification TEM image of MFN-18* nanocomposites in water. The TEM sample was prepared with NetMesh^{TM} lacey formvar stabilized with carbon copper grid. The completely open holes structure with no film support was observed.

S6. Case-study of Manganese Oxide Nanoparticles: MOP-5 and MON-5

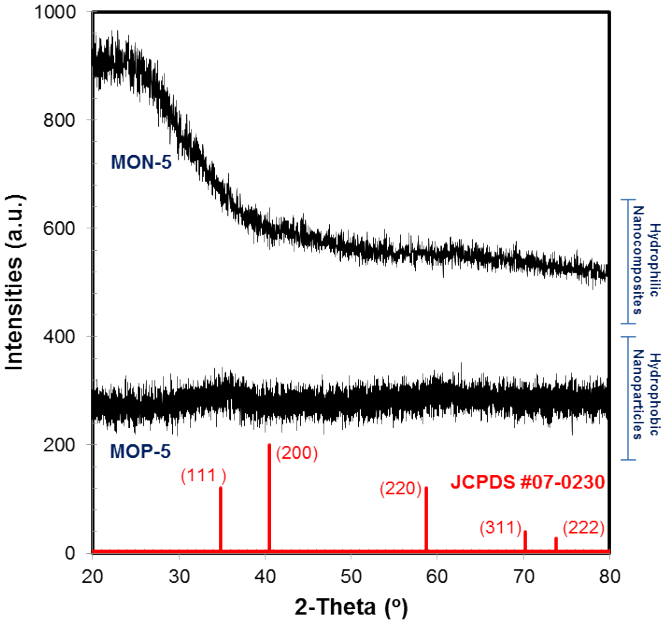

Fig. S11 XRD patterns of (bottom) hydrophobic MOP-5 and (top) hydrophilic MON-5 nanocomposite.

The typical oleic-acid coated manganese oxide nanoparticles (5 nm in size, MOP-5) were synthesized through the thermal decomposition of manganese acetate precursors in the presence of oleic acid surfactant and 1-octadecene solvent. The TEM image of the MOP-5 in $CHCl_3$ was given in **Fig. 10a**. After water solubilization with GO sheets following the DSE protocols, the water-soluble nanocomposites MON-5 were formed and stable in water phase. The TEM image of MON-5 nanocomposites in water was given in **Fig. 10b**. The XRD patterns of hydrophobic MOP-5 nanoparticles and hydrophilic MON-5 nanocomposites were summarized in **Fig. S11**. The characteristic peaks of manganese oxide nanoparticles were not clearly observed due to severe broadening effects as a result of the small MOP-5 nanoparticles size (4–5 nm).

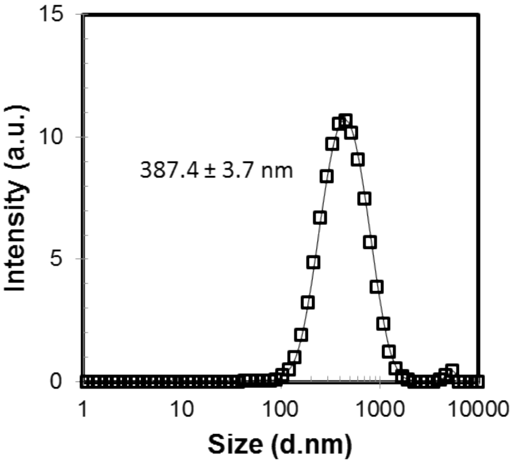

Fig. S12 Hydrodynamic size distribution of MON-5 in water at 25°C from DLS measurement.

The MR relaxivity measurement of MON-5 sample in water indicated r_1 and r_2 values of 16.1 mM $[Mn]^{-1}s^{-1}$ and 232.7 mM $[Mn]^{-1}s^{-1}$, respectively (see **Fig. 10c**). The calculated r_2/r_1 ratio was rather low (r_2/r_1 = ~14.5) as compared to the r_2/r_1 ratio of MFN-18 nanocomposites in water. The hysteresis loop of MON-5 sample given in **Fig. 10d** indicated that the nanocomposites still exhibited paramagnetism despite the aggregation observed from the TEM image. The hydrodynamic size of MON-5 nanocomposite sample was 387.4 ± 3.7 nm from the DLS experiment (see **Fig. S12**).

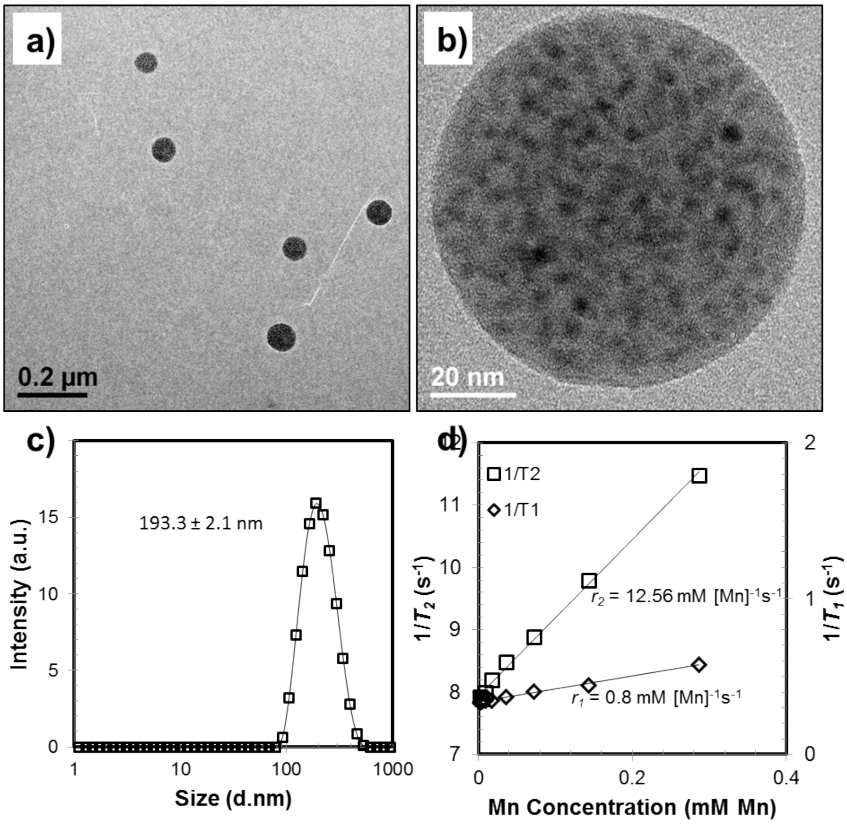

Fig. S13 (a,b) TEM images of manganese oxide nanoclusters (c-MOP-5), (c) Hydrodynamic size distribution of c-MOP-5 in water at 25°C from DLS measurement and (d) MR (T_1 and T_2) relaxivity of c-MOP-5 sample measured using Varian 7 T MRI Spectrometer.

In a control experiment, hydrophobic MOP-5 nanoparticles were also phase-transferred using PIMA-*g*-C_{12} amphiphilic brush copolymers, following previously published protocols [4]. The resultant water-dispersible c-MOP-5 nanocomposites were spherical in morphology as observed from the TEM images presented in **Fig. S13a,b**. From **Fig. S13b**, the d_{hyd} of c-MOP-5 was 193.3 ± 2.1 nm, almost half of the d_{hyd} of MON-5 nanocomposites (see **Fig. S12**). The plot of T_1 and T_2 relaxation times for c-MOP-5 samples were summarized in **Fig. S13d**. For this sample, the MR relaxivity measurement indicated that the calculated r_1 and r_2 values were rather low, especially as compared to MON-5 samples, at 0.8 mM $[Mn]^{-1}s^{-1}$ and 12.56 mM $[Mn]^{-1}s^{-1}$ respectively. The calculated r_2/r_1 ratio for c-MOP-5 sample (r_2/r_1 =

~15.1) was also slightly higher than the r_2/r_1 ratio of MON-5 sample (r_2/r_1 = ~14.5). From this comparison, it was clearly demonstrated that the GO structure provided hydrophilic environment that promoted the relaxometric properties of embedded MOP. Meanwhile, the spherical clusters of MOP-5 nanocomposites comprised of hydrophobic region within the centre of the nanoclusters that impeded water penetration, thus preventing water interaction with the inner embedded MOP-5 core.

Reference

1. D. R. Dreyer, S. Park, C. W. Bielawski and R. S. Ruoff, *Chemical Society Reviews*, 2010, 39, 228-240.
2. Y. Liu, T. Chen, C. Wu, L. Qiu, R. Hu, J. Li, S. Cansiz, L. Zhang, C. Cui, G. Zhu, M. You, T. Zhang and W. Tan, *Journal of the American Chemical Society*, 2014, 136, 12552-12555.
3. E. Peng, E. S. G. Choo, P. Chandrasekharan, C.-T. Yang, J. Ding, K.-H. Chuang and J. M. Xue, *Small*, 2012, 8, 3620-3630.
4. E. S. Guang Choo, X. Tang, Y. Sheng, B. Shuter and J. Xue, *Journal of Materials Chemistry*, 2011, 21, 2310-2319.